Supplementary information

Nickel hexacyanocobaltate quantum dots embedded in N-doped carbon for aqueous alkaline battery with ultrahigh durability

Yanhong Li[a*], Zhiting Song[a], Qifeng Zhang[a], Kai Shu[a], Hongming Hu[a], Yi Lu[a], Xiao Tang[a], Xianju Zhou[a], Xijun Wei[b], Yunhuai Zhang[c*]

[a]*College of Science, Chongqing University of Posts and Telecommunications, Chongqing, 400065, P. R. China.*

[b]*State Key Laboratory of Environment-Friendly Energy Materials, School of Materials Science and Engineering, Southwest University of Science and Technology, Mianyang, 621010, P. R. China*

[c]*College of Chemistry and Chemical Engineering, School of Materials Science and Engineering, Chongqing Univeristy, Chongqing, 400044, P. R. China*

**Corresponding Author's Email: liyanhong@cqupt.edu.cn*

xp2031@163.com

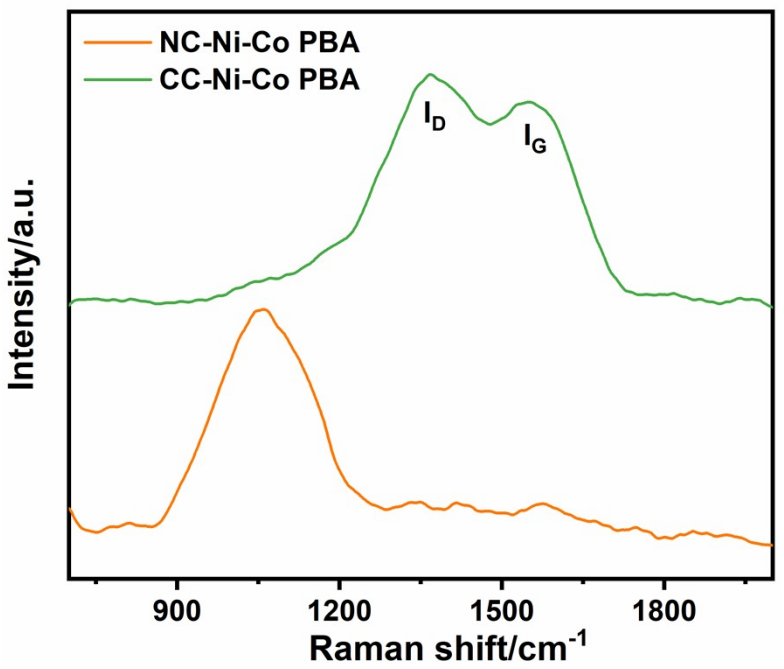

Fig. S1 Raman results of samples

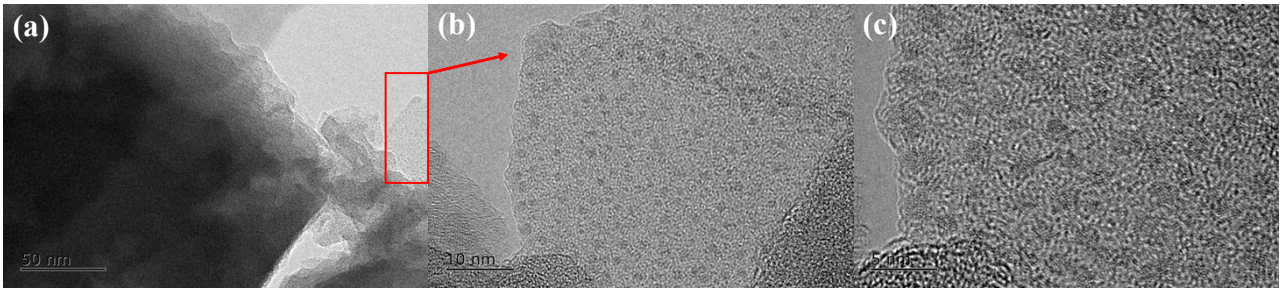

Fig. S2 TEM results of CC-Ni-Co PBA. (b) and (c) HRTEM images

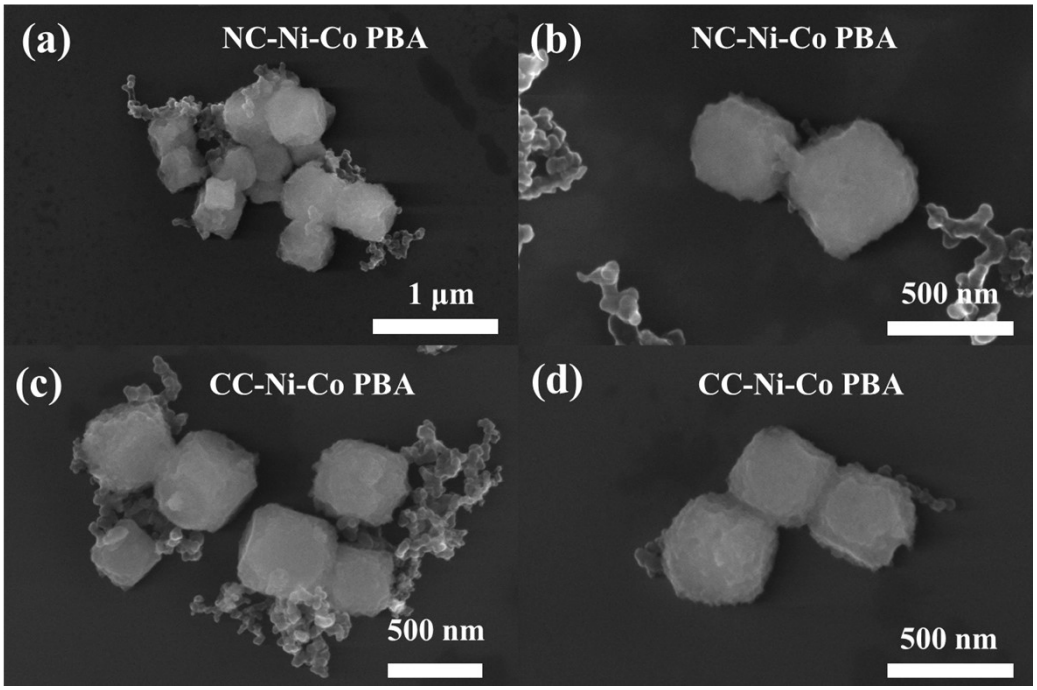

Fig. S3 SEM images of NC-Ni-Co PBA and CC-Ni-Co PBA after cycling tests

It could be seen that after cycling tests, NC-Ni-Co PBA and CC-Ni-Co PBA exhibited similar morphologies with sheet-like structures on the edges, which was typical morphological features of nickel (oxy)-hydroxides.

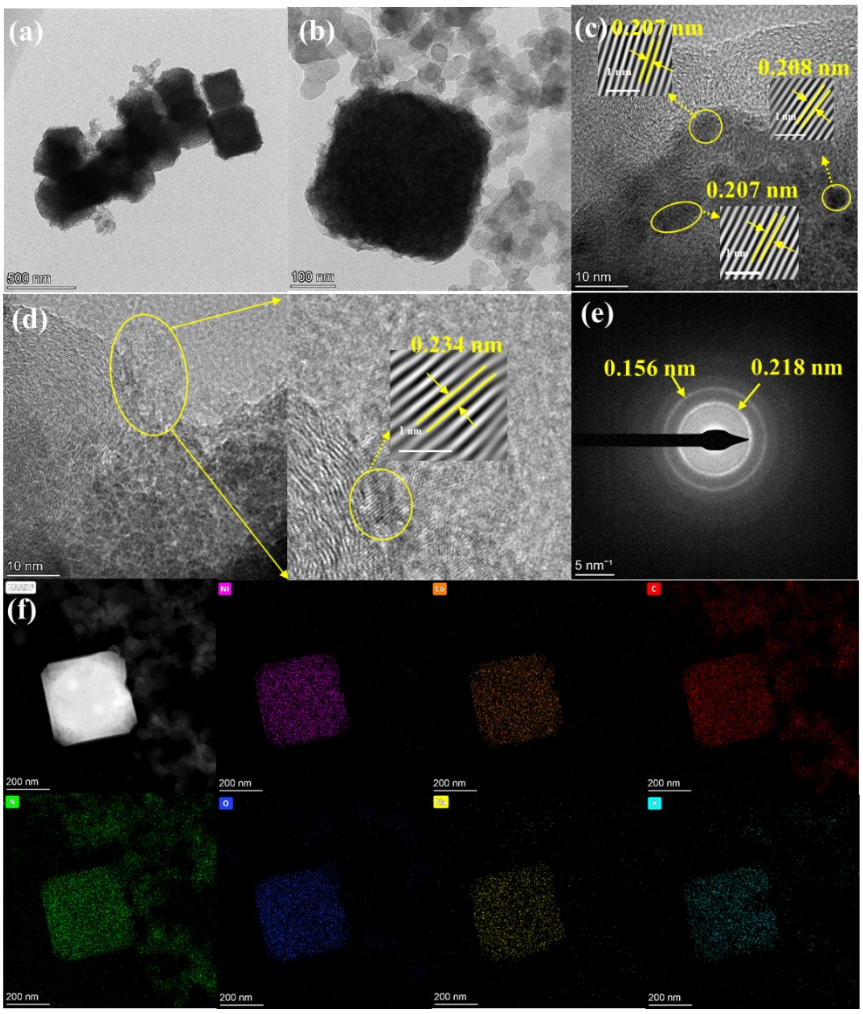

Fig. S4 TEM results of NC-Ni-Co PBA after cycling tests

TEM was conducted after cycling test to further confirm the phase transformation. We chose NC-Ni-Co PBA for TEM test. The HRTEM images in Fig. 2c showed lattice spacings of 0.207 nm and 0.208 nm, corresponding to the (422) plane of Ni-Co PBA. The existence of $Ni(OH)_2$ was confirmed by the enlarged HRTEM image of Fig. 2d and the SAED result. The lattice spacing of 0.234 nm in Fig. 2d could be assigned to (101) plane of $Ni(OH)_2$. The SAED result displayed diffraction rings with 0.156 nm and 0.218 nm, respectively, corresponding to the (110) plane of $Ni(OH)_2$ (PDF No. 14-0017) and (104) plane of NiOOH (PDF No. 06-0075), respectively.

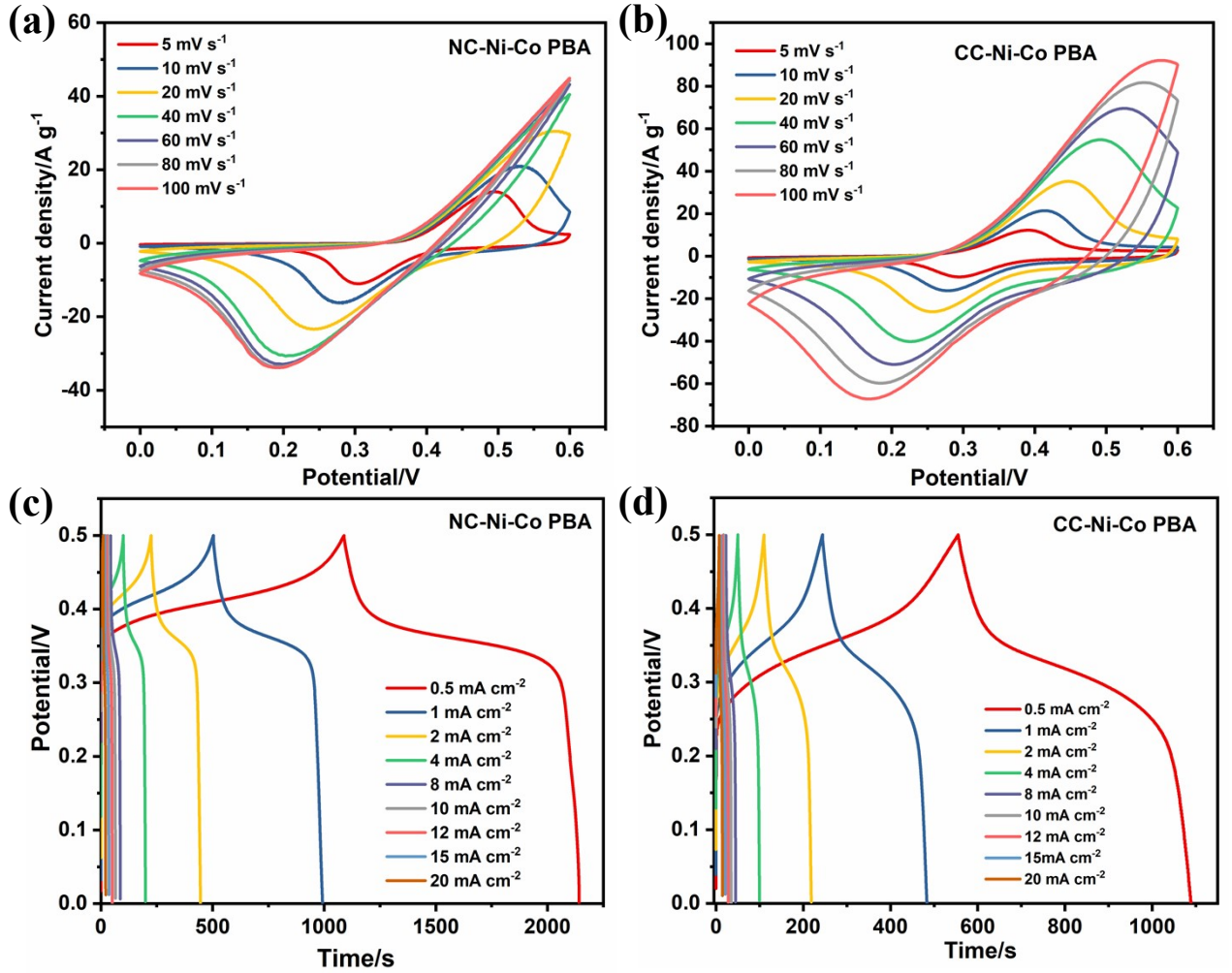

Fig. S5 (a) and (b) CV curves of samples at various scan rates; (c) and (d) GCD curves of samples under various current densities

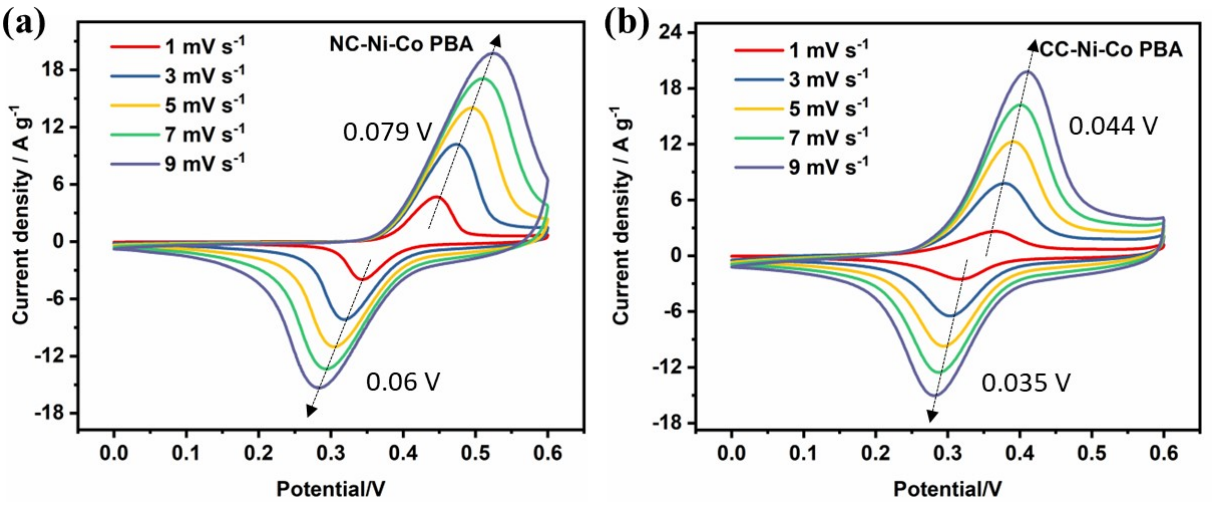

Fig. S6 CV curves of samples at different scan rates. The difference of oxidation and redox peaks potential are given.

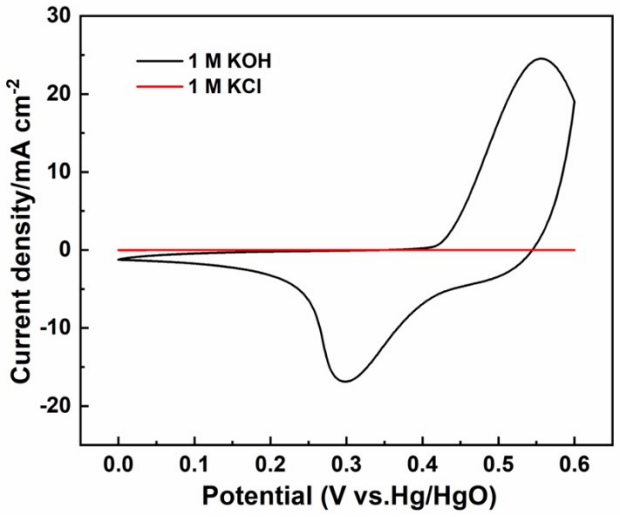

Fig. S7 CV curves of NC-Ni-Co PBA in 1M KOH and 1M KCl.

To further confirm the energy storage mechanism of Ni-Co PBA, we conducted CV test in 1M KOH and 1M KCl and the results were shown in Fig. S7. Obviously, Ni-Co PBA showed obvious oxidation and reduction peaks in KOH, while, no current signal was observed in KCl. The results indicated that the energy storage mechanism originated from the redox reaction between Ni-Co PBA and OH^-. Moreover, as previously discussed, corresponding nickel hydroxide and oxyhydroxides would inevitably be generated under such condition and the redox peaks were attributed to the reversible reaction between Ni^{2+}/Ni^{3+}.

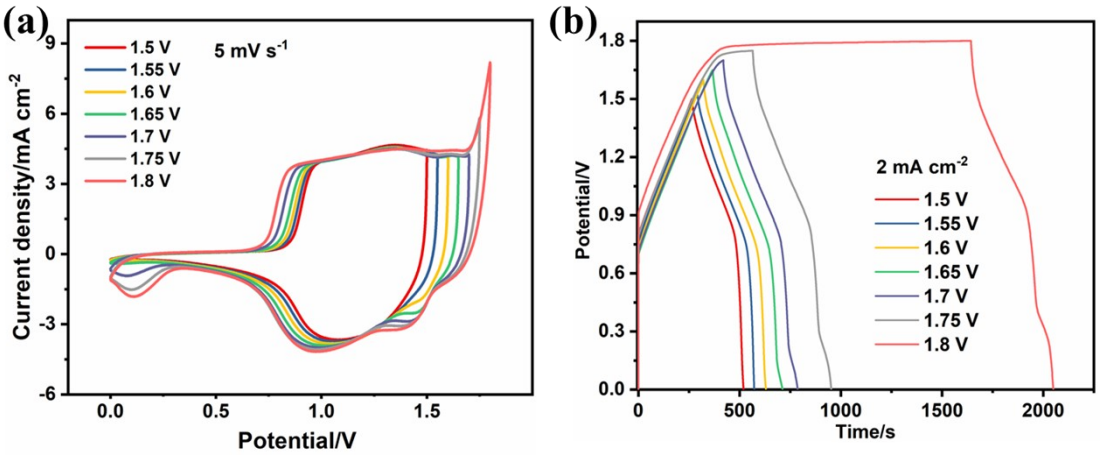

Fig. S8 CV and GCD curves of the device

Table S1 XPS fitting parameters and results of CC-Ni-Co PBA and NC-Ni-Co PBA

Sample / Fitting peaks	CC-Ni-Co PBA/eV	NC-Ni-Co PBA/eV
Ni^{2+} $2p_{3/2}$	855.8	855.95
Ni^{3+} $2p_{3/2}$	856.6	857.32
Ni^{2+} $2p_{1/2}$	873.1	873.67
Ni^{3+} $2p_{1/2}$	874.6	875.21
Co^{3+} $2p_{3/2}$	780.38	781.14
Co^{2+} $2p_{3/2}$	781.85	781.51
Co^{3+} $2p_{1/2}$	795.3	795.99
Co^{2+} $2p_{1/2}$	796.9	796.78
Metal-O	529.32	531.57
O/surface hydroxyl group	531.12	532.57
O/crystal water H_2O	533.53	/
Absorbed oxygen	532.21	533.24
C≡N/Pyridinic N	398.45	397.98
Pyrrolic N	399.95	/
C-C	284.8	284.8
C≡N	285.5	286.15
C=O	287.7	288.2